Advanced Physics Lab I

Lab Report #1 Dynamics of Rotational Motion

Group 1
Luka Burduli, Noah Horne

16.09.2024

Dr. Veit Wagner
Tim Jesko Söcker

We hereby declare that we (Luka Burduli and Noah Horne) are the sole authors of this lab report and have not used any sources other than those listed in the bibliography and identified as references throughout the report.

_____ _____

Contents

1 Abstract

The following investigation aims to calculate the moment of inertia of a gyroscopic disk I_z about its polar axis through the examination of various properties of its behavior. Additionally, the role of friction on the disk is observed, and the Coriolis force is qualitatively examined. The value of the I_z calculated solely via it's geometry was $0.00997 \pm 0.2.4 \cdot 10^{-4} kgm^2$. For calculations of the moment of inertia, our values obtained via a falling mass—30.13g, 60.13g, 90.13g—producing a torque are given as: $0.013974 \pm 4.7 \cdot 10^{-5}$, $0.01113 \pm 3.8 \cdot 10^{-4}$, $0.00961 \pm 5.6 \cdot 10^{-4}$, calculated via light gate, and $0.01427 \pm 6 \cdot 10^{-4}$, $0.01137 \pm 4.7 \cdot 10^{-4}$, $0.00941 \pm 3.3 \cdot 10^{-4}$ calculated via qualitative video analysis, all kgm^2 respectively. The values obtained via gyroscopic precession for masses 30.13g and 50.13g are: $0.01738 \pm 3.2 \cdot 10^{-3} kgm^2$ and $0.0154 \pm 2.4 \cdot 10^{-3} kgm^2$ respectively. All other observations were qualitative and lack numerical expression.

2 Introduction

For the scope of this investigation, a specific idealized class of objects called rigid bodies will be examined. By analyzing the relationship between specific rotational quantities such as angular velocity ω_r and precessional velocity ω_p and their associated periods T_r and T_p, the moment of inertia I for a gyroscopic disk is calculated along its rotational axis. Furthermore, this investigation qualitatively examines the Coriolis force exerted on an object in a rotating non-inertial reference frame.

To begin, a rigid body is an object which cannot vibrate or deform in any manner. One can describe the complete state of rigid body by stating its position $\vec{s}$ of its center of mass, and its rotation, $\vec{\phi}$. Each of these quantities also has its first and second time-derivative counterpart, velocity and angular velocity, $\vec{v} = \frac{d\vec{s}}{dt}$ and $\vec{\omega} = \frac{d\vec{\phi}}{dt}$, and angular and translational acceleration, $\vec{\alpha} = \frac{d^2\vec{\phi}}{dt^2}$ and $\vec{a} = \frac{d^2\vec{s}}{dt^2}$ respectively. It is important to note that the vectors denoting rotations are 'pseudo-vectors', pointing along the axis of rotation of the object with an associated magnitude. For every rotational axis of a rigid body, there exists an intrinsic property of the rigid body called its moment of inertia I, which can be thought of lightly as the rotational equivalent of the mass of an object in the context of its rotational dynamics. The moment of inertia about the polar axis of a gyroscopic disk M (as used throughout the investigation) characterized by volume V is defined as:

$$I_z = \int_M r^2 dm = \int_V r^2 \rho_{gd} dv \tag{1}$$

Where ρ_{gd} is the density kgm^-3 of the gyroscopic disk, integrated over the entire volume. Expressing the volume as a triple integral in cylindrical coordinates, one can rewrite it as:

$$I_z = \int_0^{d_{gd}} \int_0^{2\pi} \int_0^{r_{gd}} \left(r^3 \cdot \rho_{gd}\right) dr d\phi dz$$

$$I_z = \frac{\pi}{2} \cdot \rho_{gd} \cdot r_{gd}^4 \cdot d_{gd} \tag{2}$$

Equation 2 above represents the polar moment of inertia I_z for a disk with density ρ_{gd} radius r_{gd}, and thickness d_{gd}. Using these measurements, one can empirically determine the polar moment of inertia solely through measurements of the disk's geometry. While this method works to determine a theoretical value, it assumes an ideal cylindrical geometry which is not consistent with the real world. To more accurately determine the polar moment of inertia I_z, one can analyze the disks angular acceleration α with respect to a fixed acceleration a applied as a torque τ tangent to the circumference of the disk via a falling mass m. To apply a consistent torque to the disk, the mass m is fixed by a thread and wound around a drum on the gyroscope. This mass then produces a tension force F_s as it falls from a height h, causing a torque τ to be exerted on the disk. It is clear by the conservation of energy that the potential energy of the mass m will be completely converted into the kinetic energy of the falling mass and the rotational kinetic energy of the disk once the mass m hits the ground. By equating the potential energy of the mass with the kinetic energy of the disk and the mass, one achieves:

$$mgh = \frac{1}{2} m v_{max}^2 + \frac{1}{2} I_z \omega_{max}^2$$

This can then be rewritten into a final equation relating h and ω_{max}^2 :

$$h = \frac{mr^2 + I_z}{2mg} \omega_{max}^2 \tag{3}$$

Above denotes an alternate expression 3 for the moment of inertia I_z–while useful, its application is limited to when the slope of a graph formed by h and ω_{max}^2 is known. An alternative expression for I_z relies on the concept of gyroscopic precession to determine the moment of inertia. This alternative formalism allows a relationship between the period of rotation and precession to be established in order to compute the polar moment of inertia. This may be favorable as an alternative method to validate the results gained via the use of equation 3.

Gyroscopic precession refers to a phenomenon mediated by the conservation of angular momentum $\vec{L}$ and occurs when an external torque is orthogonally applied to the axis of rotation of a spinning rigid body. The angular momentum $\vec{L}$ of a rigid body is given by:

$$\vec{L} = I\vec{\omega} \tag{4}$$

By applying an orthogonal torque $\vec{\tau}$ to a rotating rigid body with angular momentum $\vec{L}_r$ via a small mass m' at distance r' from its center, the small change in momentum $d\vec{L}$ causes

a shift of $d\phi_p$ on the axis orthogonal to the polar axis. As this change in angle $d\phi$ is orthogonal to the angular momentum $\vec{L}_r$, the change in angular momentum $|dL_r|$ is also orthogonal to the angular momentum $\vec{L}_r$. This torque $\vec{\tau}$ is written as,

$$\vec{\tau} = m'gr' = \left|\frac{d\vec{L}}{dt}\right| \tag{5}$$

and the relationship between $d\phi_p$, $d\vec{L}_r$ and $\vec{L}_r$ is algebraically expressed as:

$$d\phi_p = \frac{|d\vec{L}_r|}{|L_r|} \tag{6}$$

Decorating both sides of the equation 6 with the time differential dt, one can transform both sides into time derivative dependent expressions, and solve for the angular velocity of precession ω_p by substituting in 4 and 5:

$$\omega_p = \frac{d\phi_p}{dt} = \frac{1}{L_r}\left|\frac{d\vec{L}}{dt}\right| = \frac{1}{I_z\omega_r}|\vec{\tau}| = \frac{m'gr'}{I_z\omega_r} \implies \underline{\underline{\omega_p = \frac{m'gr'}{I_z\omega_r}}} \tag{7}$$

By making a small substitution to replace the angular velocities with the periods of rotation–which are more easily measured experimentally–we arrive at an extremely applicable formula which describes the relationship between the period of rotation of a rigid body T_r, and its precessional period T_p under a torque $\vec{\tau}$:

$$\text{Using } \omega_p = \frac{2\pi}{T_p} \text{ and } \omega_r = \frac{2\pi}{T_r} \tag{8}$$

$$\frac{1}{T_r} = \frac{m'gr'}{4\pi^2} \cdot \frac{1}{I_z}T_p \tag{9}$$

From the equation 9 above, it is clear that there exists a directly proportional relationship between the inverse of the rotational period, $1/T_r$ and the precessional period T_p. The investigation will measure this relationship to determine the moment of inertia by solving for I_z after knowing all other constants through empirical measurements.

Lastly, this investigation qualitatively focuses on a widely known phenomenon in rotational dynamics: the Coriolis Force, or Coriolis Acceleration. The Coriolis Force is virtual force experienced by objects that exist in a non-inertial rotating reference frame. As an object moves farther or closer to the axis of rotation, it experiences an 'acceleration' perpendicular to its direction of travel. This acceleration in the rotating reference frame is caused by the relative increase of tangential velocity as an object moves farther away from the center of rotation. Moving in a straight line relative to an outside observer, by the time an object starts at the center of rotation and reaches the outer edge the rotating frame will have undergone some rotation; causing it to appear as a force to an observer in the non-inertial reference frame. The deviation

can be expressed formulaically as:

$$y = v_0 \omega t^2, \text{ assuming a constant acceleration in the non-inertial RF, } y = \frac{1}{2} a t^2$$

$$\implies a = 2\omega v_0$$

Applyings Newton's Second Law to this acceleration (the Coriolis Acceleration), and taking into account the direction of travel of the projectile, we arrive at a final formula which describes the Coriolis Force F_C.

$$F_C = ma = 2 \cdot m \cdot \omega \cdot v_0 \cdot \sin \alpha \qquad \alpha \text{ is the angle between } \vec{v}_0 \wedge \vec{\omega}. \tag{10}$$

With equations 1-12, a sufficient level of theory can be applied during the investigation and analysis of the data collected during our experimental procedure.

3 Experimental Procedure

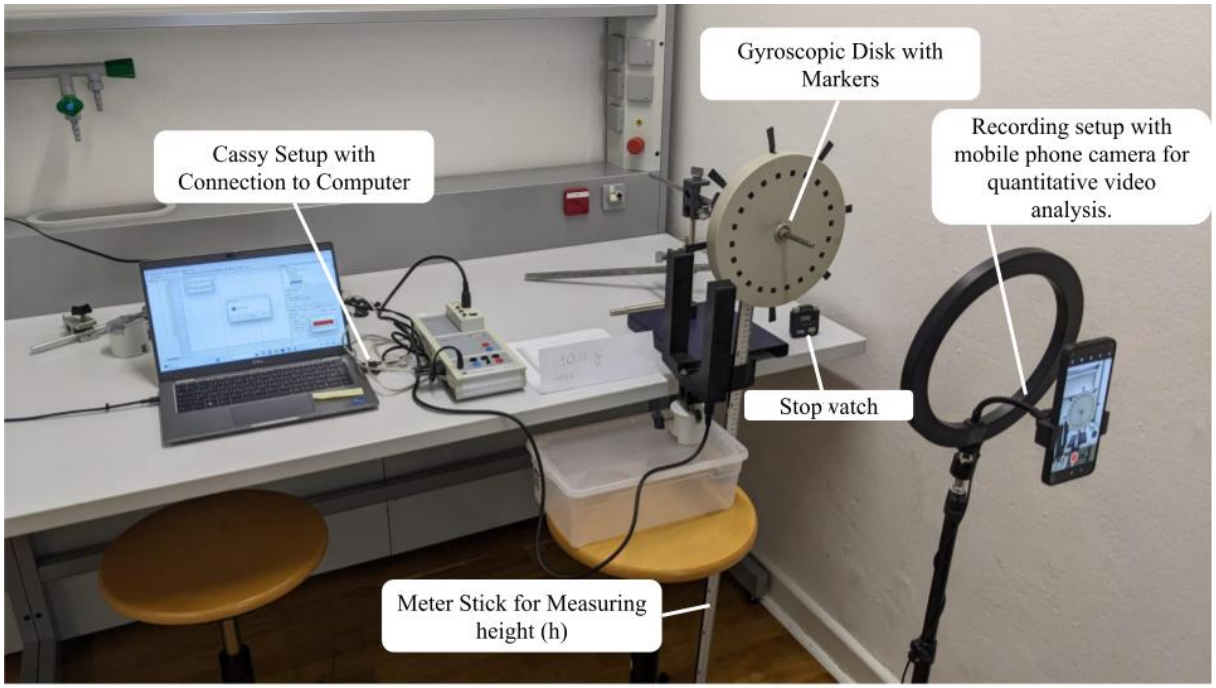

Figure 1: Experimental Setup for Gravitational Calculation of I_z

First, one can determine the theoretical value of the moment of inertia by measuring the radius, thickness, and density of the disk and substituting into formula 2. It is important to mark down uncertainties for measurements as well to correctly propagate the absolute uncertainty of the moment of inertia I_z.

After these static measurements and calculations, the first experimental setup aims to determine the moment of inertia I_z by analyzing the relationship between the height h of a dropped mass m and the maximum angular velocity of the wheel ω_{max}^2 as described in equation 3. The mass m is attached via a string to the axle of the gyroscopic disk pictured above. By attaching light blocking appendages about the circumference of the disk (divided into 8 equal placements), a light gate helps measure an 8-th of the rotational period of the disk. Connecting this light gate to a CASSY and running it into the CASSY data processing software on the computer, one can easily determine the maximum square of angular velocity ω_{max}^2 achieved by the falling mass by finding the minimum 8-th of a period $T_{min}/8$. The minimum period yields the maximum angular velocity as the two quantities are related via $T_{min} = 2\pi/\omega_{max}$. 5 measurements are taken for each of the 7 distinct heights–ranging every 5cm from 70cm to 40cm–for each of the 3 masses (30g, 60g and 90g). A total of 105 measurements will be taken. In each measurement, one notes down the minimum period $T_{min}/8$ measured by the CASSY, and uses it as raw data, marking down the height and weight of the mass used. By plotting the results after calculating ω_{max}^2 from the periods, the moment of inertia I_z can be found by equating the slope of the resultant graph to the coefficient of ω_{max}^2 in equation 3. As a further investigation into this same phenomena, a similar plot will be made by extracting ω_{max}^2 through quantitative video (60FPS) analysis, performed by a Python software using OpenCV. By recording the spinning disk, we can track the angle of rotation of the disk using black markers stuck to the front of the disk for each frame, and measuring the discrete angular velocity via the following equation 11:

$$\omega = \frac{\Delta\phi}{\Delta t}, \text{ for each frame.} \tag{11}$$

For the second part of the investigation, the friction present in the disk is analyzed by measuring the change in period T_r and angular velocity ω_r over time. Due to the velocity dependent nature of friction, it is predicted that one should observe an exponential increase and exponential decrease for the period and angular velocity respectively (see below):

$$m\frac{d\omega}{dt} = -mk\omega \implies \frac{1}{\omega}d\omega = -kdt \implies \omega = C_1 e^{-kt} \tag{12}$$

After using the CASSY to measure the period until the disk comes to a stop, plot the measurements on a graph, and calculate the unknown coefficients for k and C_1, the coefficients of friction. By fitting an inverse exponential curve to the angular velocity, the linear dependence of the friction acceleration with respect to angular velocity (equation 12) is proven.

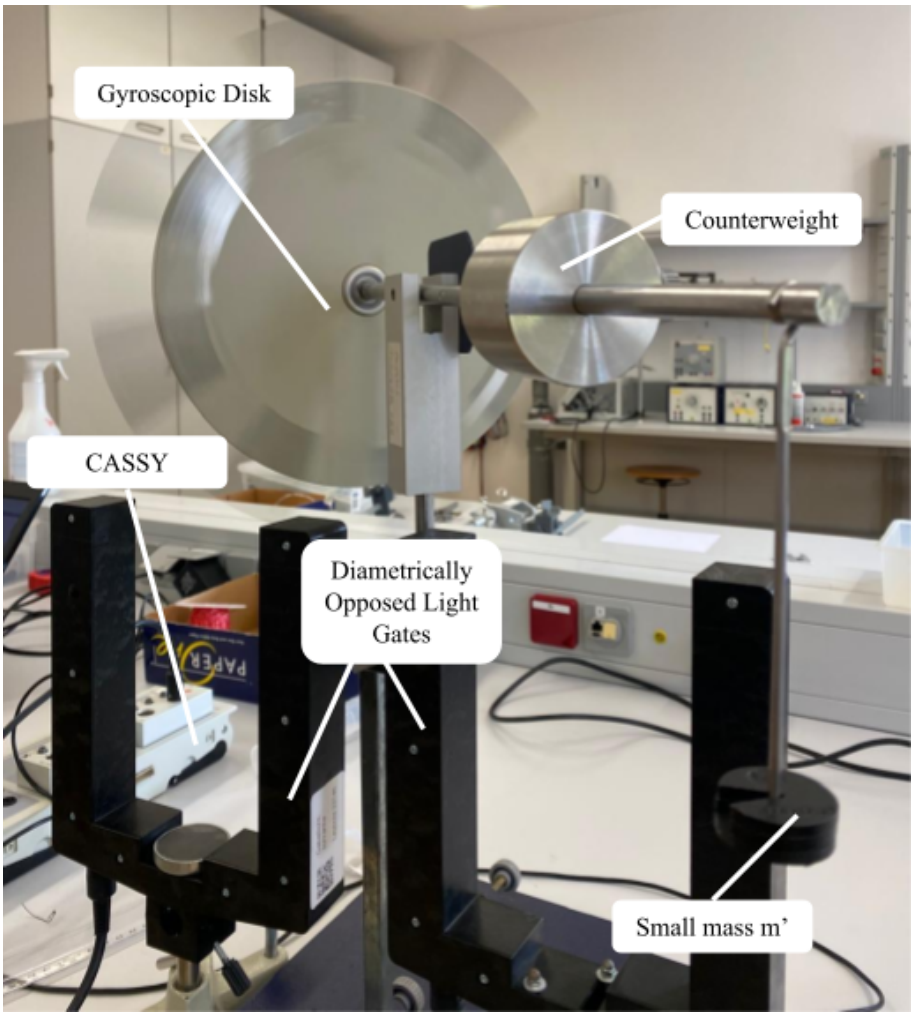

Figure 2: Experimental Setup for Precessional Calculation of I_z

As a third method for calculating the moment of inertia I_z, we can use the theory developed by equation 9 and measure the relationship between the inverse rotational period of precession T_p, and the rotational period of the disk T_r. Similar to how a light gate was used as a measure of the period for the first setup, the next setup requires the use of two light gates (Figure 2). Each light gate is positioned diametrically opposed to the other, and one more axis of the gyroscopic disk is let free to allow an orthogonal torque to be placed on the axle to precess the disk horizontally. This axle has a length r', and is measured before measurement begins. A counterweight is used to create a torque equilibrium across the non-polar axis of rotation, so that a very small mass m' can be added to produce a small torque. A mass of 30g and 50g are used, and for each mass 6 measurements are taken for both the rotational angular velocity ω_r and the precessional angular velocity ω_p. As the disk passes through each light gate, the rotational period is given via $T_r/8$, and the time taken for the disk to rotate between one light gate and the other gives $T_p/2$. These measurements can then be modified to give $1/T_r$ and T_p, which are consequently plotted on a graph to determine a slope, which is then equated to the coefficient of T_p in equation 9 to calculate the polar moment of inertia through gyroscopic precession.

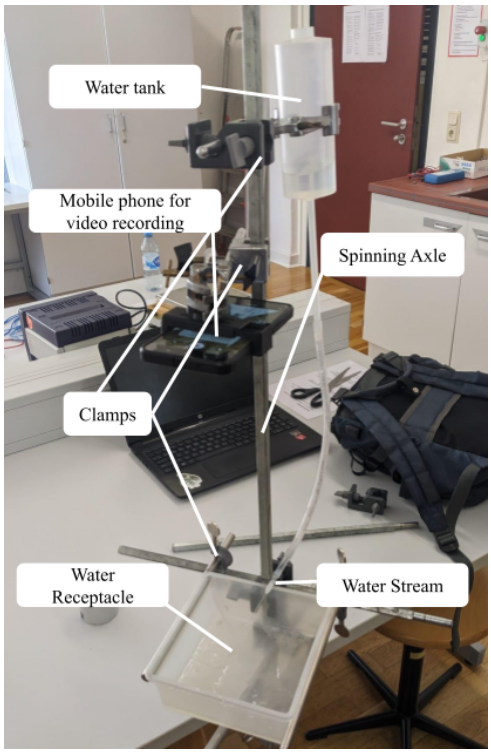

Figure 3: Experimental Setup for Qualitative Observation of the Coriolis Force

The last component of this investigation focuses on the qualitative analysis of the Coriolis Force. For this setup, a tube of water is positioned to project water over a receptacle tub placed all anchored to a spinning vertical axle. For visualization purposes, a mobile phone was also anchored to the spinning axis to help visualize the perspective on an observer in the rotating inertial reference frame and clearly view the trajectory of the water for both clockwise and counterclockwise rotations (Figure 3).

4 Results and Data Analysis

The values below denote the raw data gathered regarding the geometry of the gyroscopic disk. These values are consequently used everywhere in the processing of the moment of inertia as important constants–mass m_{gd}, radius r_{gd}, thickness d_{gd}, volume V_{gd} and density ρ_{gd}.

- Mass m_{gd} (kg) = 1.32858 ± 0.0001 kg
- Radius r_{gd} (m) = 0.1225 ± 0.0005 m
- Thickness d_{gd} (m) = $(2.8 \pm 0.05) \cdot 10^{-2}$ m
- Volume V_{gd} = $\pi r_{gd}^2 d_{gd} = (1.32 \pm 0.026) \cdot 10^{-3}$ m^3
- Density ρ_{gd} = $\frac{m_{gd}}{V_{gd}}$ = 1006 ± 20 kgm^{-3}

With just these values, one can arrive at the first physically meaningful result of this investigation, a theoretical calculation of the moment of inertia through its geometrical parameters. Substituting the above constants into equation 2, one achieves:

$$I_z = \frac{\pi}{2} \cdot (1006) \cdot (0.1225)^4 \cdot (2.8 \cdot 10^{-2}) \approx 0.00997 \pm 0.00024 \text{ kgm}^2 \tag{13}$$

Throughout the investigation, one can compare their calculated results to the theoretical geometrically computed value as a means of verifying the validity and consistency of results. The first major statistical result derived from this investigation is the calculated moment of inertia via the linear relationship between the height h of an attached mass m and the maximum angular velocity ω_{max}^2 exhibited by the gyroscopic disk as a result of the masses' gravitational acceleration g. 3 masses were used across 7 different heights with 5 trials each, below the raw data is tabulated.

Table 1: Raw data collected by light gate for measurement of relationship between w_maxˆ2 and h. (M = 30.13 +- 0.01 g)

h (meters)	T_min/8 (sec)					mean T_min/8	(error) T_min/8	(mean) T_min	(error) T_min	(mean) w_maxˆ2
0.7	0.144	0.144	0.142	0.144	0.143	0.1434	0.00018	1.1472	0.0014	29.9973
0.665	0.147	0.144	0.144	0.146	0.145	0.1452	0.00026	1.1616	0.0021	29.2581
0.6	0.15	0.149	0.15	0.15	0.149	0.1496	0.00011	1.1968	0.00088	27.5623
0.55	0.159	0.163	0.16	0.158	0.161	0.1602	0.00038	1.2816	0.0031	24.03559
0.5	0.17	0.165	0.166	0.166	0.165	0.1664	0.00041	1.3312	0.0033	22.2778
0.45	0.174	0.176	0.173	0.173	0.174	0.1740	0.00024	1.3920	0.0020	20.3742
0.4	0.182	0.186	0.18	0.183	0.183	0.1828	0.00043	1.4624	0.0035	18.4598

Table 2: Raw data collected by light gate for measurement of relationship between w_maxˆ2 and h. (Mass = 60.13 +- 0.01 g)

h (meters)	T_min/8 (sec)					mean T_min/8	(error) T_min/8	(mean) T_min	(error) T_min	(mean) w_maxˆ2
0.7	0.095	0.093	0.094	0.094	0.093	0.0938	0.00017	0.7504	0.0013	70.10905059
0.665	0.095	0.096	0.095	0.094	0.096	0.0952	0.00017	0.7616	0.0013	68.06218168
0.6	0.099	0.102	0.1	0.1	0.098	0.0998	0.0003	0.7984	0.0024	61.93250982
0.55	0.106	0.106	0.102	0.104	0.104	0.1044	0.00033	0.8352	0.0027	56.59509137
0.5	0.109	0.108	0.109	0.109	0.108	0.1086	0.00011	0.8688	0.0009	52.30221868
0.45	0.117	0.117	0.118	0.112	0.118	0.1164	0.0005	0.9312	0.004	45.5274999
0.4	0.122	0.12	0.122	0.121	0.122	0.1214	0.00018	0.9712	0.0014	41.85452227

Table 3: Raw data collected by light gate for measurement of relationship between w_maxˆ2 and h. (Mass = 90.13 +- 0.01 g)

h (meters)	T_min/8 (sec)					mean T_min/8	(error) T_min/8	(mean) T_min	(error) T_min	(mean) w_maxˆ2
0.7	0.072	0.074	0.073	0.074	0.072	0.073	0.0002	0.584	0.0016	115.7534763
0.665	0.075	0.077	0.081	0.073	0.076	0.0764	0.00059	0.6112	0.0047	105.6800586
0.6	0.08	0.079	0.077	0.078	0.079	0.0786	0.00023	0.6288	0.0018	99.84691954
0.55	0.082	0.085	0.083	0.084	0.083	0.0834	0.00023	0.6672	0.00182	88.68448767
0.5	0.083	0.086	0.087	0.086	0.086	0.0856	0.0003	0.6848	0.0024	84.18451872
0.45	0.093	0.089	0.091	0.09	0.091	0.0908	0.0003	0.7264	0.0027	74.81833956
0.4	0.093	0.098	0.099	0.098	0.098	0.0972	0.00048	0.7776	0.0038	65.29008483

Let us perform a sample calculation to quickly derive the ω_{max}^2 from a data set of values for $T_{min}/8$. Using the example for a height h of 0.7 meters, one can immediately determine the arithmetic mean by summing all values and dividing by 5. Then one applies formula 8 after multiplying the average value for $T_{min}/8$ by 8.

$$\text{For } h = 0.7m, T_{min}/8 = 0.073s \implies T_{min} = 0.584s \implies \omega_{max}^2 = \left(\frac{2\pi}{T_{min}}\right)^2 \approx 115.75 \text{rad}^2\,\text{s}^{-2}$$

Plotting the height dropped against the maximum square of the angular velocity ω_{max}^2, a linear trend $h \propto \omega_{max}^2$ should be observed, and from it, the moment of inertia I_z extracted. Below are the graphs illustrating this proportional relationship for masses 30.13g, 60.13g, and 90.13g respectively.

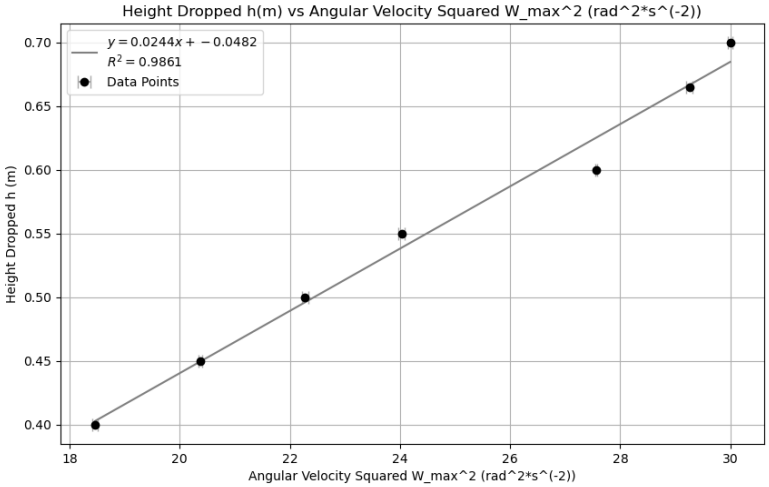

Figure 4: Plot of Height Dropped (h) against ω_{max}^2 for m = 30.13g

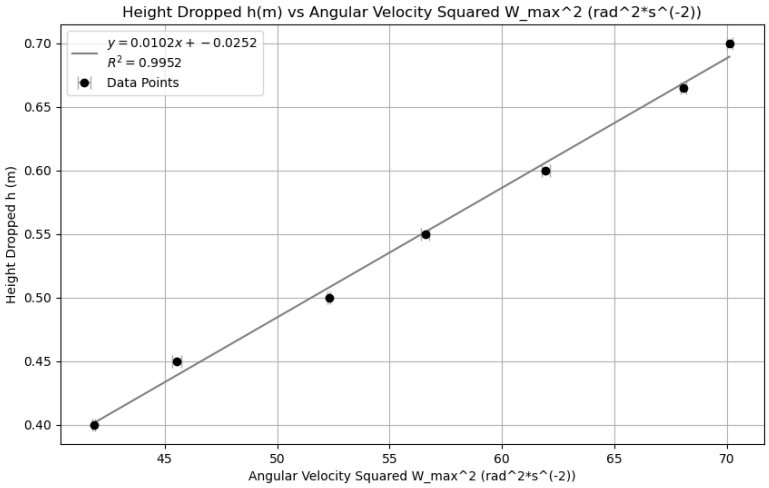

Figure 5: Plot of Height Dropped (h) against ω_{max}^2 for m = 60.13g

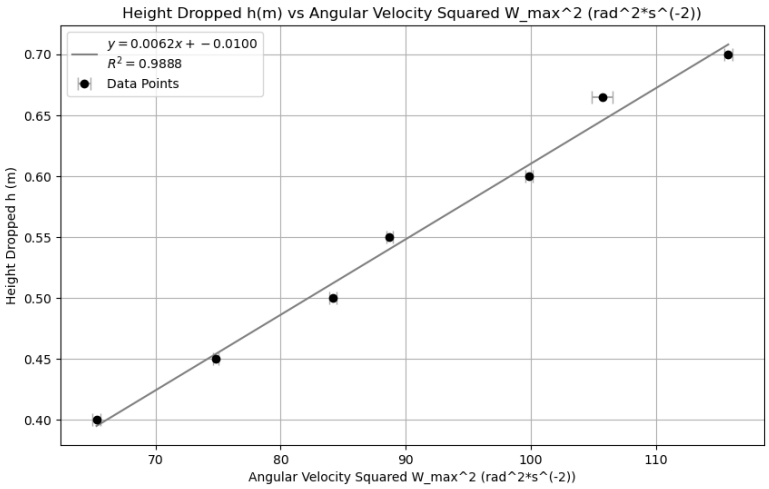

Figure 6: Plot of Height Dropped (h) against ω_{max}^2 for m = 90.13g

As one can observe, the graphs demonstrate a strong positive linear correlation for each set of data values. It is important to note that although the error bars are present in the graph, they are very small due to the relative magnitude of the absolute error to the data points. The vertical error bars are given by the instrumental uncertainty of the measured height, and the horizontal error bars were calculated by propagating the error of T_{min}, such that:

$$\Delta\omega_{max}^2 = \Delta\left(\frac{2\pi}{T_{min}}\right)^2 = \left|\frac{\Delta T_{min}}{T_{min}}\right| \cdot \frac{4\pi}{T_{min}} \tag{14}$$

For each mass, the associated graph of h against ω_{max} has a slope k with its absolute uncertainty determined formulaically using the correlation coefficient R^2 in the graph with the following formula:

$$\Delta k = m\sqrt{\frac{(1/R^2) - 1}{n-2}} \tag{15}$$

Calculating the uncertainties for the slopes, the slopes are given by:

1. $k_{30.13g} = (2.44 \pm 0.13) \cdot 10^{-2}$ m rad^{-2} s^2
2. $k_{60.13g} = (1.02 \pm 0.032) \cdot 10^{-2}$ m rad^{-2} s^2
3. $k_{90.13g} = (6.2 \pm 0.29) \cdot 10^{-3}$ m rad^{-2} s^2

With these values, the moment of inertia I_z can be calculated by equating the slope k to the coefficient of ω_{max} in formula 3, rearranging the terms, an expression for I_z is acquired in terms of known constants, and the slope k; below is the derivation to reach 16.

$$h = \frac{mr^2 + I_z}{2mg}\omega_{max}^2 \implies k = \frac{mr^2 + I_z}{2mg} \implies 2mgk - mr^2 = I_z$$

$$I_z = 2mgk - mr^2 \tag{16}$$

For each of the slopes above, one can substitute the values of m, r and k to get the moment of inertia I_z.

$$\text{Case m=30.13g} \implies I_z = 2(30.13 \cdot 10^{-3})(9.81)(2.44 \cdot 10^{-2}) - (30.13 \cdot 10^{-3})(0.1225)^2$$

$$\implies I_{z(30.13g)} = 0.013974 \pm 4.7 \cdot 10^{-5} kgm^2$$

$$\text{Case m=60.13g} \implies I_z = 2(60.13 \cdot 10^{-3})(9.81)(0.0102) - (60.13 \cdot 10^{-3})(0.1225)^2$$

$$\implies I_{z(60.13g)} = 0.01113 \pm 3.8 \cdot 10^{-4} kgm^2$$

$$\text{Case m=90.13g} \implies I_z = 2(90.13 \cdot 10^{-3})(9.81)(6.2 \cdot 10^{-}3) - (90.13 \cdot 10^{-3})(0.1225)^2$$

$$\implies I_{z(90.13g)} = 0.00961 \pm 5.2 \cdot 10^{-4} kgm^2$$

The errors for the moments of inertia were calculated through the root sum of squares method, a partial derivative error propagation method that will be covered during the Error Analysis section. As an alternative way to demonstrate this relationship, quantitative video analysis was employed to find the maximum angular velocity of the wheel, and consequently, the similar relationship observed in the graphs above. Below shows the information extracted from the video analysis for ω^2_{max}, for each height.

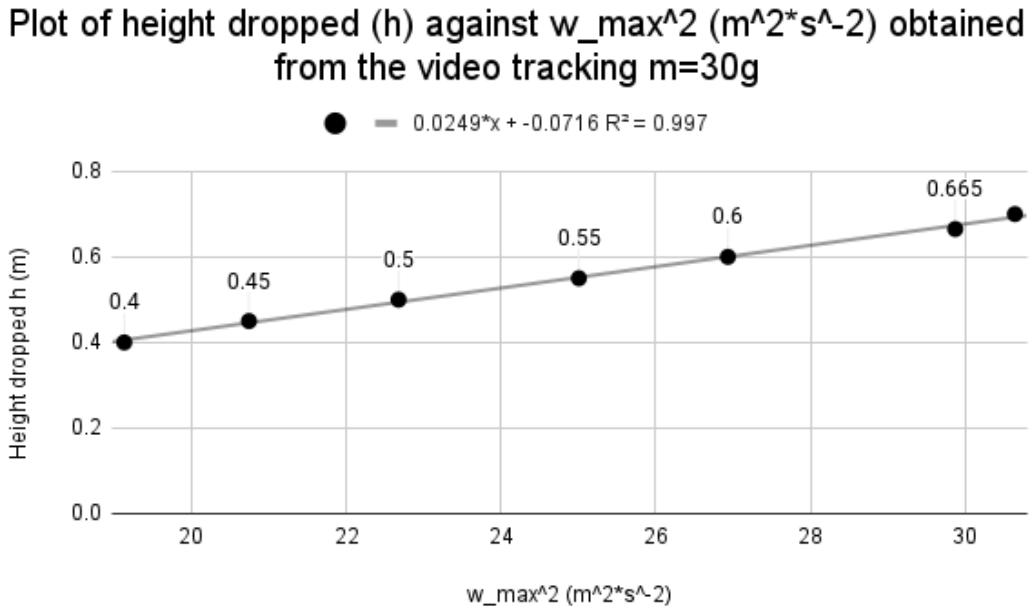

Figure 7: Plot of Height Dropped (h) against ω^2_{max} for m = 30.13g

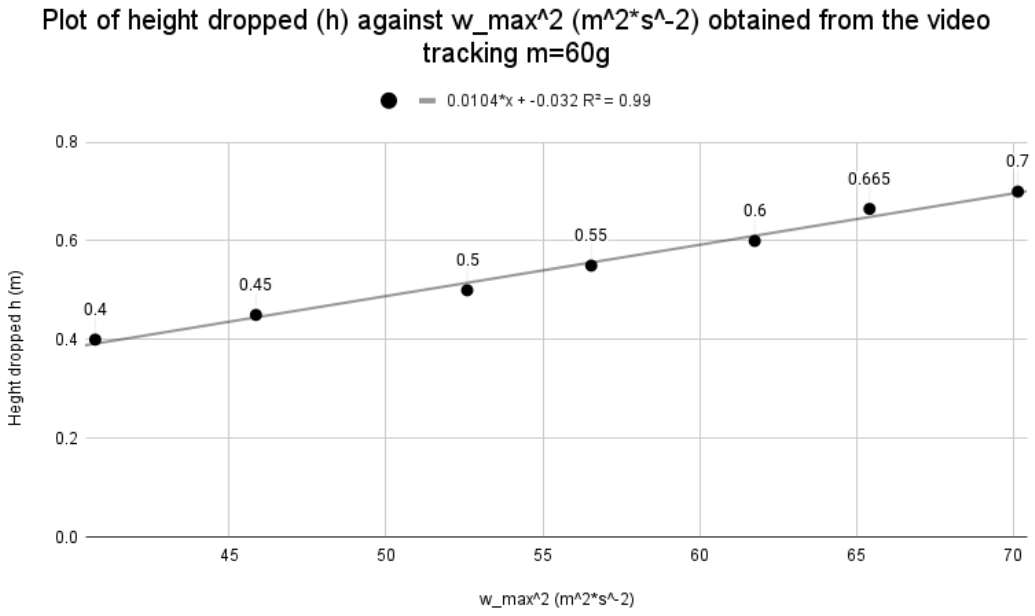

Figure 8: Plot of Height Dropped (h) against ω_{max}^2 for m = 60.13g

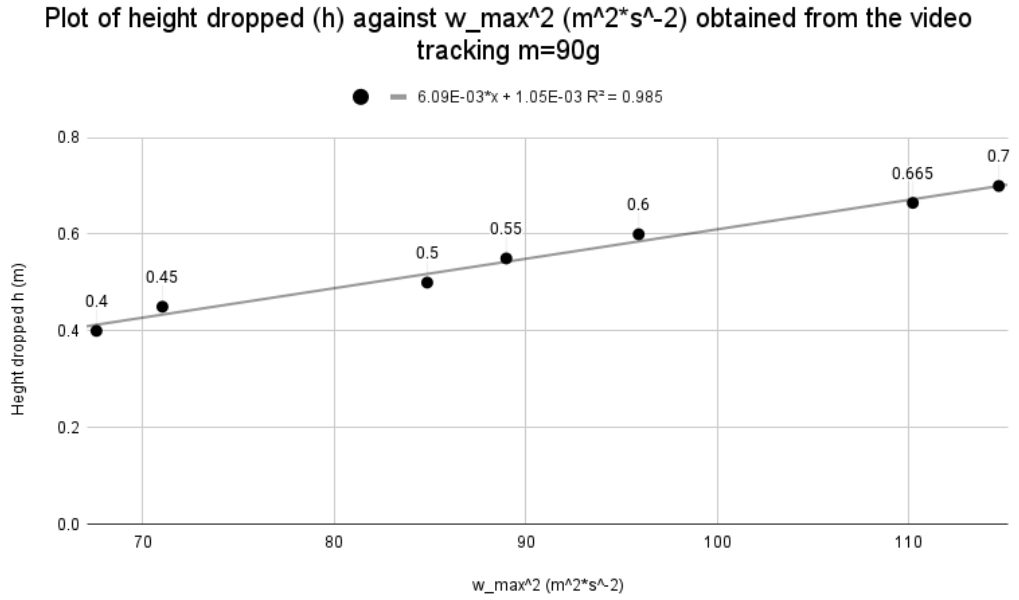

Figure 9: Plot of Height Dropped (h) against ω_{max}^2 for m = 90.13g

As one can see, a very similar trend appears. This is expected, as the same phenomena is observed, simply through a different instrumentation. Using the slopes of these graphs, one employs the same formula 16 using the slopes of the graphs above to yield 3 more values for the moment of inertia.

$$\text{Case m=30.13g} \implies I_z = 2(30.13 \cdot 10^{-3})(9.81)(0.0249 \cdot 10^{-2}) - (30.13 \cdot 10^{-3})(0.1225)^2$$

$$\implies I_{z(30.13g)} = 0.01427 \pm 6 \cdot 10^{-4} kgm^2$$

$$\text{Case m=60.13g} \implies I_z = 2(60.13 \cdot 10^{-3})(9.81)(0.0104) - (60.13 \cdot 10^{-3})(0.1225)^2$$

$$\implies I_{z(60.13g)} = 0.01137 \pm 4.7 \cdot 10^{-4} kgm^2$$

$$\text{Case m=90.13g} \implies I_z = 2(90.13 \cdot 10^{-3})(9.81)(6.1 \cdot 10^{-}3) - (90.13 \cdot 10^{-3})(0.1225)^2$$

$$\implies I_{z(90.13g)} = 0.00941 \pm 3.3 \cdot 10^{-4} kgm^2$$

The next phenomena subject to investigation is the effect of rotational friction on the angular velocity and period of the rotating gyroscopic disk. As the data is collected over a large time interval, the data will not be included as a table, rather solely through graphical representation of the results. Below denotes the readings of the sensor for the period of rotation T_r and the angular velocity against time.

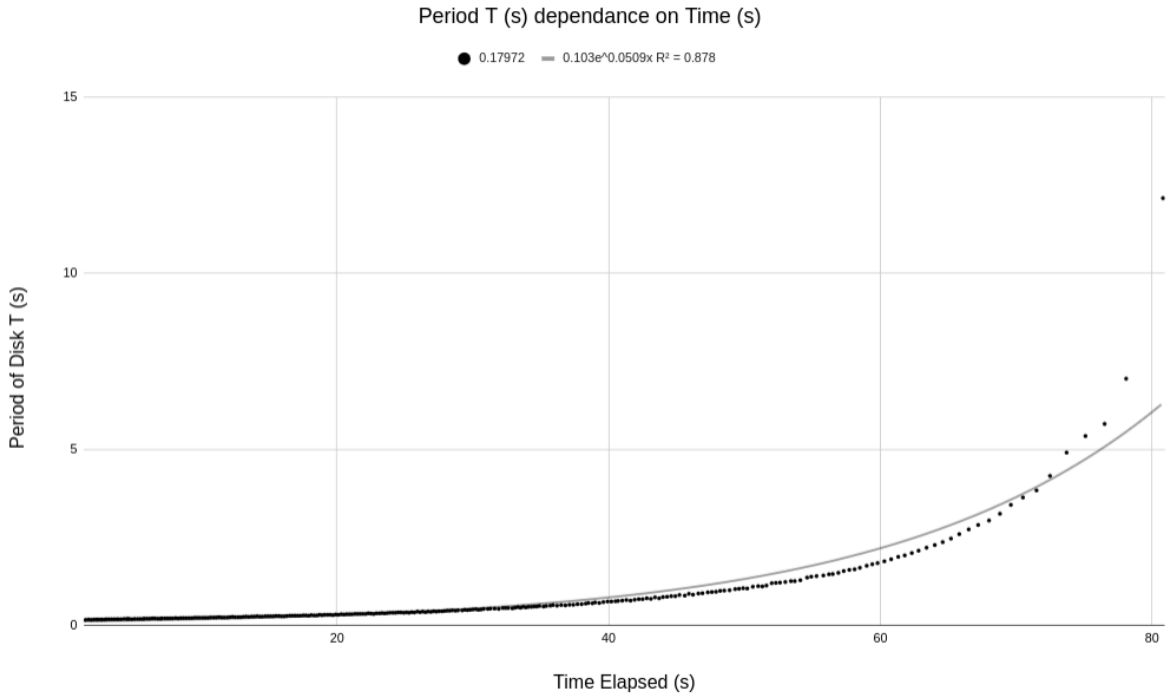

Figure 10: Plot of the Period of Rotation T_r against time (t)

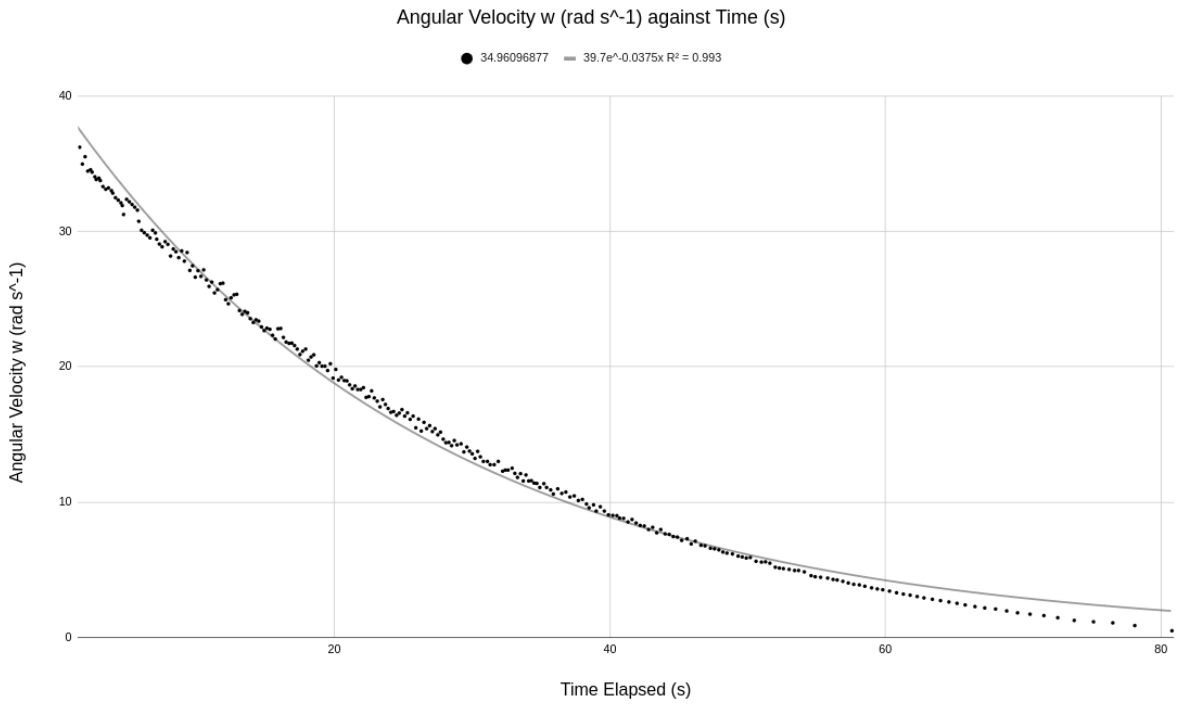

Figure 11: Plot of the Rotational Angular Velocity ω_r against time (t)

As one can see, a clear exponential increase and decay can be observed, which is consistent with the theory developed in the introduction, where the ODE was solved to show exponential behavior (See formula 12).

Moving further into the investigation, one can examine the relationship between precessional angular velocity ω_p and rotational angular velocity ω_r for a gyroscopic disk with two free rotational axes, subject to a small mass used to create an orthogonal torque as previously discussed. The two masses used are of mass 30.13g and 50.13g respectively. It was also measured that the distance from the small mass attachment point and the non-polar axis of rotation was ($\approx 0.275 \pm 0.0005m$). Below are the tables of raw data collected during the experiment:

Table 5: 1/Rotational Period vs. Precessional Period for mass 30.14g

T_r/8 Before Turn (s) +- 0.001s	T_r/8 After Turn (s) +- 0.001s	T_p/2 +- 0.002s	T_p	error of T_p	1/T_r	error 1/T_r
0.036	0.061	10.7	21.4	0.004	0.02323204163	0.038
0.03	0.073	10.6	21.2	0.004	0.02342359224	0.033
0.039	0.041	7.5	15	0.004	0.03315210184	0.055
0.053	0.064	15.5	31	0.004	0.01606270882	0.026
0.06	0.076	13.3	26.6	0.004	0.01869019139	0.019
0.028	0.075	8.7	17.4	0.004	0.02849002849	0.033

Table 6: 1/Rotational Period vs. Precessional Period for mass 50.13g						
T_r/8 Before Turn (s) +- 0.001s	T_r/8 After Turn (s) +- 0.001s	T_p/2 +- 0.002s	T_p	error of T_p	1/T_r	error 1/T_r
0.045	0.051	6.5	13	0.004	2.604166667	0.038
0.043	0.049	6	12	0.004	2.717391304	0.033
0.037	0.042	4.9	9.8	0.004	3.164556962	0.055
0.045	0.061	6.9	13.8	0.004	2.358490566	0.026
0.032	0.043	4.6	9.2	0.004	3.333333333	0.019
0.032	0.041	5.1	10.2	0.004	3.424657534	0.033

The calculations above are quite simple, just scalar multiplication or inversion of the measured values. Below demonstrates the plots of the precessional period T_p against the inverse of the rotational period $1/T_r$.

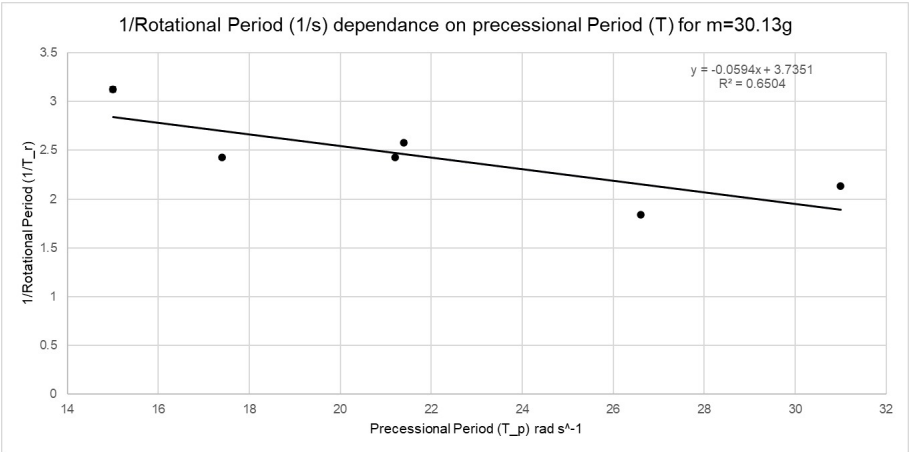

Figure 12: Plot of the precessional period T_p against the inverse of the rotational period $1/T_r$

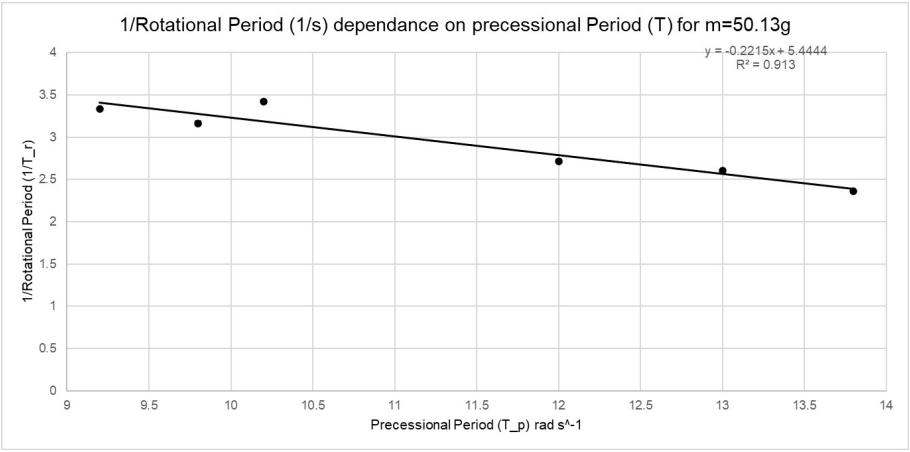

Figure 13: Plot of the precessional period T_p against the inverse of the rotational period $1/T_r$

As one can observe in the graphs, a clear negative linear relationship is present. The value of the slope k can be similarly equated to the coefficient of T_p in formula 9 to find the moment of inertia I_z. Below is the derivation of the expression for the moment of inertia I_z.

$$\frac{1}{T_p} = \frac{m'gr'}{4\pi^2} \cdot \frac{1}{I_z} T_p \implies k = \frac{m'gr'}{4\pi^2} \cdot \frac{1}{I_z} \implies I_z = \frac{m'gr'}{4\pi^2 k}$$

Given that the values of the slope for a mass of 30.13 and 50.13 grams are known, one can calculate the moment of inertia in a similar way, including its associated error. The error is propagated using the root sum of squares method as mentioned before. Furthermore, the error of the slope is calculated using formula 15. Below are the calculated values of the moment of inertia I_z with their associated absolute uncertainties.

Case where mass = 30.13g $\implies I_z = \dfrac{(30.13 \cdot 10^-3)(-9.81)(0.275)}{4\pi^2(-0.119)} \approx 0.01738 \pm 3.2 \cdot 10^{-3} kgm^2$

$$\implies I_{z(30.13g)} = 0.01738 \pm 3.2 \cdot 10^{-3} kgm^2$$

Case where mass = 50.13 $\implies I_z = \dfrac{(50.13 \cdot 10^-3)(-9.81)(0.275)}{4\pi^2(-0.221)} \approx 0.0154 \pm 2.4 \cdot 10^{-3} kgm^2$

$$\implies I_{z(50.13g)} = 0.0154 \pm 2.4 \cdot 10^{-3} kgm^2$$

These values are statistically similar to the theoretically calculated moment of inertia I_z as well as the ω^2_{max} calculated moments of inertia, neither deviating from one another by more than $0.01 kgm^2$.

The last aspect of the investigation focuses on qualitatively analyzing the behavior of a water stream in a rotating reference frame, and observing the Coriolis force. Below are photos illustrating the behavior of the water stream (taken through anchored phone) for clockwise rotation, counterclockwise rotation and no rotation respectively.

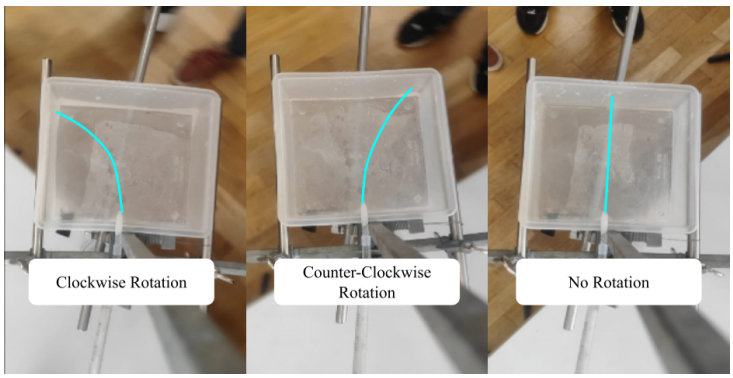

Figure 14: Qualitative Depiction of the Coriolis Force for Jet of Water

As one can observe, a clockwise rotation creates a virtual force which acts on the stream of water to the left as it moves forward away from the axis of rotation. As the translational velocity of the outer edge is much greater than the translational velocity at the axis of rotation, this change in relative translational velocity results in an acceleration, which we can see above. Likewise, for a counterclockwise rotation, the water stream veers to the right, a result of the change in translational velocity as the water moves away from the axis of rotation. Naturally also, when the stream is no longer rotating, the water moves straight as no tangent force is acting upon it. It was also noticed that for faster angular velocities, the curve was more emphasized, a direct result of the greater acceleration caused by a faster rotation. This dependence is nicely formulaically described by equation 10—as ω increases, F_C increases, validating the results of the investigation.

5 Error Analysis

There were many potential sources of error present during this experiment that may have introduced error into the measurements. These sources of error include: parallax error, friction of the axle, and negligence of string mass. Parallax error was easily mitigated by aligning the eyes of the experimenter to be level with the ruler, however as the mass required free space as to not collide with anything during its descent, it proved difficult to be exact as a result. As empirically observed in Figure 13, friction is present on the axle. This led to an additional acceleratory torque opposite to that created by the mass, shifting the results slightly for ω_{max}. Note also that due to the variance in height for each measurement, this systematic error is likely difficult to control. Third, the mass of the string was assumed to be negligible. While albeit the entire mass of the string was no more than 2 grams, on the scale of mass used–masses of 30 grams–2 grams added to the weight could lead to a maximal $\approx 2/30 = 0.0666 \approx 6.6\%$ deviation of the masses actual value used, yet another systematic error, dependent on height. To calculate the propagated error of significant results such as the moment of inertia I_z, the square root of the sum of squares method (RSS) was used. Below denotes the formula for the propagated error of a calculated value Δy in terms of n uncertain parameters x_i with absolute uncertainties Δx_i.

$$\Delta y = \sqrt{\sum_{i=0}^{n} \left(\frac{\partial y}{\partial x_i} \cdot \Delta x_i \right)^2} = \sqrt{\left(\frac{\partial y}{\partial x_1} \cdot \Delta x_1 \right)^2 + \cdots + \left(\frac{\partial y}{\partial x_n} \cdot \Delta x_n \right)^2} \tag{17}$$

As a sample calculation to demonstrate this formula, the absolute propagated uncertainty of the moment of inertia ΔI_z derived from geometric measurements (see 2).

$$\Delta I_z = \sqrt{\left(\frac{\pi}{2} r_{gd}^4 d_{gd} \cdot \Delta \rho_{gd} \right)^2 + \left(2\pi r_{gd}^3 \rho_{gd} d_{gd} \cdot \Delta r_{gd} \right)^2 + \left(\frac{\pi}{2} \rho_{gd} r_{gd}^4 \cdot \Delta d_{gd} \right)^2} \tag{18}$$

Substituting in the measured values, the absolute uncertainty is easily obtained. This error propagation method was used for every formulaic description of the moment of inertia due to its widespread versatility.

During the scenarios in which the formula for the absolute uncertainty of the moment of inertia depends on the slope, formula 15 was applied, using the R^2 value calculated by the regression software. While for the aspects of the experiment using the light gate connected to the CASSY as the primary measurement instrument had a small digital uncertainty, it was important to likewise calculate the absolute uncertainty of the angular velocity given that the video software analyzed the footage at 60fps.

For the error analysis of the qualitative video analysis, an alternative absolute error was used. To calculate our values for the angular velocity, we had to perform the measurements in a step-wise fashion to accommodate for the type of data given. To perform the error analysis for the quantitative video analysis of the rotational velocity ω, variables involved are defined:

- ϕ_1 and ϕ_2: Angular positions of the disk at times t_1 and t_2, respectively.
- $\Delta\phi_1$=0.01 rad and $\Delta\phi_2$ =0.01 rad: Uncertainties in the angular positions ϕ_1 and ϕ_2.
- t_1 and t_2: Times corresponding to ϕ_1 and ϕ_2.
- Δt_1=1/60 sec and Δt_2=1/60 sec: Uncertainties in the times t_1 and t_2.

The rotational velocity ω is given by:

$$\omega = \frac{\phi_2 - \phi_1}{t_2 - t_1}$$

To find the uncertainty in ω ($\Delta\omega$), we consider the uncertainties in ϕ_1, ϕ_2, t_1, and t_2. These uncertainties propagate through the calculation of ω using error propagation formula 17. Using the partial derivatives and the uncertainties, we get:

$$\Delta\omega = \sqrt{\left(\frac{\Delta\phi_1}{t_2 - t_1}\right)^2 + \left(\frac{\Delta\phi_2}{t_2 - t_1}\right)^2 + \left(\frac{(\phi_2 - \phi_1)\Delta t_1}{(t_2 - t_1)^2}\right)^2 + \left(\frac{(\phi_2 - \phi_1)\Delta t_2}{(t_2 - t_1)^2}\right)^2}$$

Precessional Period (T_p) Error: The precessional period (T_p) was calculated as twice the value of $T_p/2$. Given that $T_p/2$ is substraction of two time points, and each of them has error of ± 0.001s, the error of $T_p/2$ is ± 0.002s and the error in T_p is:

$$\Delta T_p = 2 \times \Delta(T_p/2) = 2 \times 0.002\text{s} = \pm 0.004\text{s}$$

Rotational Period (T_r) Error: The rotational period T_r is calculated as:

$$T_r = 8\left(\frac{T_r/8 \text{ (Before Turn)} + T_r/8 \text{ (After Turn)}}{2}\right)$$

The uncertainty in T_r is determined using the propagation of errors for the sum and average of the two $T_r/8$ measurements, each with an uncertainty of ± 0.001s.

$$\Delta\left(T_r\right) = \frac{1}{2}\sqrt{(\Delta T_{r_1})^2 + (\Delta T_{r_2})^2}$$

1/T_r Error: The error in $\frac{1}{T_r}$ is calculated using the propagation of uncertainty for a function of the form $\frac{1}{x}$, where x has an uncertainty Δx:

$$\Delta\left(\frac{1}{T_r}\right) = \left|-\frac{1}{T_r^2}\right| \Delta T_r = \frac{\Delta T_r}{T_r^2}$$

This process is repeated for each row in the table to calculate the uncertainty in $\frac{1}{T_r}$.

Lastly, as the investigation of the Coriolis force was purely qualitative, no major error calculations were necessary for the degree of precision of the observations (purely based on direction of flow). No major errors occurred during the experiment's process, so for this setup error is not of crucial importance.

6 Discussion

Throughout the investigation, the results of each setup yielded acceptably consistent results with the relevant theory. However, limitations in the method and instrumental capabilities led to various offsets of the data. To begin, the geometrically calculated value of the moment of inertia is subject to error due to the difference in the assumed geometry of the disk, and the real world disk. While during the derivation of the geometrically calculated moment of inertia (see Formula 2) the geometry of the disk was assumed to be a perfect cylinder, the model does not take into account the additional spool where the string sits. This spool was made of a similar material and was quite large, introducing a systematic error to the calculated value.

Figure 15: Demonstration of disk geometry inconsistency

If this extra cylinder was taken into account, the moment of inertia would have been slightly larger, which would thereby be more consistent with the rest of the experimental measurements, which all deviate from the geometrically calculated value by approximately $\pm 0.03 kgm^2$. For this reason, many of the values are larger than the theoretical value and do not coincide within their uncertainty ranges.

Now, for the measurements of ω_{max}^2, the method employed was very effective and consistent. The CASSY yielded favorable measurements. The values for the moment of inertia I_z produced for each of the 3 masses (30.13g, 60.13g,90.13g) fall close together, however decrease for higher masses. Furthermore, this decrease in moment of inertia with increase in mass used is observed similarly in the results of the quantitative data analysis section. Examining the results of both methods, they are extremely coherent. This implies that there is indeed some form of systematic error which causes the calculated value of the moment of inertia to be somehow dependent on the mass that is dropped. A very good guess as to why this phenomena occurs and is consistent across both setups is axle friction. As demonstrated in the graph 13, for higher angular velocities, there is a much greater friction torque, as friction is velocity dependent. For larger masses, the overall angular acceleration of the disk is greater, causing the average angular velocity to be greater. As a direct consequence, the frictional force is greater, causing all graphs to have a lesser slope the faster the axle spins. This is a direct explanation for why larger masses have smaller moments of inertia, as a smaller slope would yield a consequently small moment of inertia (see formula 16).

As for the results calculated using the precessional velocity, there is a larger error, due to the use of two light gates, however the results are accurate to the theoretical (geometrical) value as well. Once again, the larger mass yielded a smaller moment of inertia. However, not for the same reason. As the mass does not contribute to the acceleration of the disk (which is done manually), it is likely due to the way the disk falls from the horizontal quicker with a larger mass, decreasing the horizontal component of precessional torque leading to a lesser period. As a lesser precessional period would lead to a greater slope on average, the main cause of this systematic error is clear.

As for the results of the Coriolis force setup, the qualitative observations made were very consistent with the theory; the clockwise rotation creating a force to the left, and counter-clockwise to the right (see Figure 14).

7 Conclusion

In this experiment, the moment of inertia of a gyroscopic disk through various methods was determined and the factors affecting its measurement were investigated. The methods employed included theoretical calculation based on geometric parameters, analysis of angular velocity from a dropped mass, and examination of gyroscopic precession.

The theoretical moment of inertia calculated from the geometric properties of the wheel was $0.00997 \pm 000024 kgm^2$. The experimentally obtained values were generally consistent with this theoretical value, especially for lower masses where frictional effects were less pronounced. Relationship between angular velocity and spinning wheel was determined and with two different methods (video analysis and light gate measurement) information about angular velocity was obtained.

Results obtained by light gate: $I_{z(30.13g)} = 0.013974 \pm 4.7 \cdot 10^{-5} kgm^2$, $I_{z(60.13g)} = 0.01113 \pm 3.8 \cdot 10^{-4} kgm^2$, $I_{z(90.13g)} = 0.00961 \pm 5.2 \cdot 10^{-4} kgm^2$.

Results obtained by video analysis:$I_{z(30.13g)} = 0.01427 \pm 6 \cdot 10^{-4} kgm^2$, $I_{z(60.13g)} = 0.01137 \pm 4.7 \cdot 10^{-4} kgm^2$, $I_{z(90.13g)} = 0.00941 \pm 3.3 \cdot 10^{-4} kgm^2$.

Additionally relationship between precessional period and inverse of the rotational period was found. From the slope of the graph moment of inertia was found:

$I_{z(30.13g)} = 0.01738 \pm 3.2 \cdot 10^{-3} kgm^2$ and $I_{z(50.13g)} = 0.0154 \pm 2.4 \cdot 10^{-3} kgm^2$.

Finally, the Coriolis force was investigated by observing the direction of a water stream in a rotating reference frame.

It was clear from the results that the primary source for error in this experiment were the frictional forces. To enhance the accuracy of the measurements, future experiments could involve the minimization of frictional effects, perhaps by using a low-friction bearing or conducting the experiment in a vacuum to eliminate air resistance. Ensuring minimum string slippage could also provide more accurate results, however its implications are minor. A more important improvement for this experiment would be the avoiding of small torques created by the experimenters hand when releasing the weight. By creating a machine release, this could be much more consistent, leading to less random error. Overall, the experimental results very nicely adhere to one another, and the results were accurate and precise given the experimental conditions.